Redox Biology 59 (2023) 102596

Contents lists available at ScienceDirect

Redox Biology

journal homepage: www.elsevier.com/locate/redox

Dietary and genetic disruption of hepatic methionine metabolism induce acid sphingomyelinase to promote steatohepatitis

Cristina Alarcón-Vila [a,b,c,#], Naroa Insausti-Urkia [a,b,c,#], Sandra Torres [a,b,c], Paula Segalés-Rovira [a,b,c], Laura Conde de la Rosa [a,b,c], Susana Nuñez [a,b,c], Raquel Fucho [a,b,c], Jose C. Fernández-Checa [a,b,c,d,*,1], Carmen García-Ruiz [a,b,c,d,1,**]

[a] Cell Death and Proliferation, Instituto de Investigaciones Biomédicas de Barcelona, CSIC, Barcelona, Spain
[b] Liver Unit, Hospital Clínic I Provincial, IDIBAPS, Barcelona, Spain
[c] CIBERehd, University of Barcelona, Spain
[d] University of Southern California Research Center for Liver Diseases, Keck School of Medicine, USC, Los Angeles, CA, USA

ARTICLE INFO

Keywords:
Ceramide
Methionine
Alcoholic steatohepatitis
Nonalcoholic steatohepatitis
Amitriptyline

ABSTRACT

Alcoholic (ASH) and nonalcoholic. (NASH).steatohepatitis are advanced.stages.of.fatty.liver.disease.Methionine adenosyltransferase 1A (MAT1A) plays a key role in hepatic methionine metabolism and germline *Mat1a* deletion in mice promotes NASH. Acid sphingomyelinase (ASMase) triggers hepatocellular apoptosis and liver fibrosis and has been shown to downregulate *MAT1A* expression in the context of fulminant liver failure. Given the role of ASMase in steatohepatitis development, we investigated the status of ASMase in *Mat1a*$^{-/-}$ mice and the regulation of ASMase by SAM/SAH. Consistent with its role in NASH, *Mat1a*$^{-/-}$ mice fed a choline-deficient (CD) diet exhibited macrosteatosis, inflammation, fibrosis and liver injury as well as reduced total and mitochondrial GSH levels. Our data uncovered an increased basal expression and activity of ASMase but not neutral SMase in *Mat1a*$^{-/-}$ mice, which further increased upon CD feeding. Interestingly, adenovirus-mediated shRNA expression targeting ASMase reduced ASMase activity and protected *Mat1a*$^{-/-}$ mice against CD diet-induced NASH. Similar results were observed in CD fed *Mat1a*$^{-/-}$ mice by pharmacological inhibition of ASMase with amitriptyline. Moreover, *Mat1a/ASMase* double knockout mice were resistant to CD-induced NASH. ASMase knockdown protected wild type mice against NASH induced by feeding a diet deficient in methionine and choline. Furthermore, *Mat1a*$^{-/-}$ mice developed acute-on-chronic ASH and this outcome was ameliorated by amitriptyline treatment. In vitro data in primary mouse hepatocytes revealed that decreased SAM/SAH ratio increased ASMase mRNA level and activity. *MAT1A* and *ASMase* mRNA levels exhibited an inverse correlation in liver samples from patients with ASH and NASH. Thus, disruption of methionine metabolism sensitizes to steatohepatitis by ASMase activation via decreased SAM/SAH. These findings imply that *MAT1A* deletion and ASMase activation engage in a self-sustained loop of relevance for steatohepatitis.

Abbreviations: ASMase, acid sphingomyelinase; ASH, alcoholic steatohepatitis; CD, choline deficient diet; DAG, diacylglyerol; DAPE, 1,2-diarachidoyl-sn-glycerol-3-phosphatidylethanolamine; DAPC, 1,2-diarachidoyl-sn-glycerol-3-phosphatidylocholine; MCD, methionine and choline deficient diet; MEMAPC, monoether-monoacyl-phosphatidylcholine; MEMAPE, monoether-monoacyl-phosphatidylethanolamine; NASH, nonalcoholic steatohepatitis; NPA disease, Niemann-Pick type A disease; PC, phosphatidylcholine; PE, phosphatidylethanolamine; SAM, S-adenosyl-L-methionine; SAH, S-adenosylhomocysteine; TAG, triacylglycerol.

* Corresponding author. Cell Death and Proliferation, Instituto de Investigaciones Biomédicas de Barcelona, CSIC, Barcelona, Spain
** Corresponding author. Cell Death and Proliferation, Instituto de Investigaciones Biomédicas de Barcelona, CSIC, Barcelona, Spain.
E-mail addresses: checa229@yahoo.com (J.C. Fernández-Checa), carmen.garcia@iibb.csic.es (C. García-Ruiz).
# These authors contributed equally to the work.
1 These authors share senior authorship.

https://doi.org/10.1016/j.redox.2022.102596
Received 23 December 2022; Accepted 28 December 2022
Available online 2 January 2023

1. Introduction

Steatohepatitis is an advanced stage of fatty liver disease, which can progress to cirrhosis and hepatocellular carcinoma (HCC), and is characterized by steatosis, inflammation, fibrosis and oxidative stress. Steatohepatitis encompasses both alcoholic (ASH) and nonalcoholic steatohepatitis (NASH). Although the etiology of ASH and NASH differ both exhibit common biochemical features, such as steatosis, liver injury, inflammation and fibrosis [1,2]. Therapeutic treatment for ASH and NASH is limited due to our incomplete understanding of the mechanisms underlying the transition from steatosis to steatohepatitis.

The liver plays a major role in the metabolism of methionine and disruption of this pathway is associated with chronic liver disease. Methionine uptake in the liver is metabolized to S-adenosylmethionine (SAM), which is of outmost importance for liver physiology and health. The biotransformation of methionine into SAM is catalyzed by methionine adenosyltransferases MATI/MATIII, encoded by *MAT1A*, which is expressed in adult liver [3,4]. SAM is an essential methyl donor involved in the methylation of a wide range of biomolecules, including DNA, proteins and lipids. In this regard, phosphatidylethanolamine-N-methyltransferase (PEMT) requires SAM to catalyze the methylation of phosphatidylethanolamine (PE) to generate phosphatidylcholine (PC), and hence limitation of SAM levels compromises an adequate PE/PC ratio required to ensure lipid homeostasis. Following methylation, SAM is converted into S-adenosylhomocysteine (SAH), which can be further transformed into homocysteine (Hcy). Furthermore, through its conversion into cysteine in the transsulfuration pathway, SAM is also a precursor for the synthesis of GSH, a major antioxidant defense. Impaired MATI/MATIII activity and decreased SAM/SAH are causally associated with the development of steatohepatitis [5–11]. The relevance of SAM generation by MATI/III in liver pathophysiology is best illustrated by the impact of *Mat1a* deletion in mice, which exhibited decreased SAM/SAH and developed spontaneous NASH by 9–10 months of age that progressed to HCC by 12–14 months [12]. Moreover, feeding a choline-deficient diet (CD) to wild type (WT) mice causes liver steatosis, while *Mat1a*$^{-/-}$ mice develops NASH when fed a CD diet [12].

Ceramide is a bioactive sphingolipid that regulates many cellular processes, including differentiation, metabolism and signal transduction and mediates cell death in response to stress, inflammatory cytokines and chemotherapy [13–18]. Cells generate ceramide via two major pathways. It can be synthesized *de novo* by the condensation of palmitoyl-CoA and serine in the endoplasmic reticulum (ER) or it can be generated from the hydrolysis of sphingomyelin (SM) by sphingomyelinases (SMases) [18,19]. Several SMases have been characterized, which differ in their optimum pH and intracellular site of activation [20,21]. Among SMases, the acid sphingomyelinase (ASMase), which is encoded by *SMPD1*, encompasses a lysosomal ASMase and a secretory Zn^{2+}-dependent isoform and has been shown to promote steatosis, hepatocellular apoptosis and liver fibrosis [22–26]. Moreover, ASMase mediates alcohol and high fat diet-induced ER stress and regulates lysosomal membrane permeabilization [24–26]. Of relevance, a functional relationship between MATI/III and ASMase has been described in the context of fulminant liver failure induced by TNF. In this paradigm, ASMase-induced ceramide generation leads to *MAT1A* mRNA decay, resulting in MATI/III downregulation, hepatic SAM depletion and sensitization to TNF-induced lethal hepatitis [27].

Given the role of ASMase in steatohepatitis development [24–26,28], the purpose of the present study was to investigate the status of *ASMase* expression in *Mat1a*$^{-/-}$ mice and the regulation of *ASMase* by different concentrations of SAM and SAH. Our findings indicate that dietary or genetic disruption of methionine metabolism sensitizes to steatohepatitis by ASMase activation via decreased SAM/SAH. Moreover, patients with ASH and NASH exhibit an inverse correlation between *MAT1A* and *ASMase* expression, suggesting that *MAT1A* deletion and ASMase activation engage in a self-sustained loop of relevance for steatohepatitis.

2. Materials and methods

2.1. *Mat1a*$^{-/-}$, *ASMase*$^{-/-}$ and double *Mat1a/ASMase* knockout mice

C57BL/6J male mice were purchased from Charles River. *MAT1a*$^{-/-}$, and *ASMase*$^{-/-}$ mice were previously generated and characterized [12,23–25]. Double *Mat1a/ASMase* mice (C57BL/6J strain) were generated by crossing *Mat1a*$^{-/-}$ mice and *ASMase*$^{+/-}$ mice and genotyped, as previously described [12,29]. 8 weeks old *Mat1a*$^{-/-}$, ASMase$^{-/-}$ and double *Mat1a/ASMase* knockout mice and their littermates were used in the present study and subjected to diet-induced NASH and ASH.

2.2. Nutritional NASH and ASH

For diet-induced NASH animals were fed a control diet (Teklad, cat no: 2914) or a CD diet (Research Diets, cat no: D05010401) for 14 days. In some cases, wild type mice were fed a MCD diet (Research Diets, cat no: A02082002B) for up to 14 days. The daily intake of the different diets was comparable (110–120 mg/g of body weight per day). For diet-induced ASH model, animals were subjected to the acute-on-chronic NIAAA model and pair fed a control (Ctrl) or ethanol-containing (EtOH) Lieber-De Carli liquid diets (Research Diets, cat no: L10016A), providing 36% of calories from ethanol (or maltose), as previously described [30]. After 10 days of chronic alcohol feeding, mice were gavaged with alcohol (5 g/kg) and sacrificed 8 h later. In some cases, animals were injected i.p. daily with amitriptyline (5 mg/kg/day, dissolved in saline, Sigma Aldrich) for the 14 days or treated by intravenous tail injection with an adenovirus targeting ASMase (5×10^7pfu/g, dissolved in saline up to 100 μL) for the last 7 days of CD diet feeding. Animals were housed in temperature-and humidity-controlled rooms and kept on a 12 h light/dark cycle. All the experimental protocols used were approved and performed in accordance with the Animal Care Committee of the Hospital Clinic-Universidad de Barcelona and conformed to the highest international standards of humane care of animals in biomedical research. Sample processing for analyses is described in supplementary methods.

2.3. Samples from human ASH and NASH and real time PCR

Human liver samples were obtained from liver explants of patients diagnosed with NASH and ASH undergoing liver transplantation. The clinical data of the patients are presented in Supplementary Table 1. In addition, normal liver tissue was obtained from the surgical specimen of donor livers used for transplantation. The protocol was approved by the Hospital Clinic/UB Ethics Committee. All controls had normal serum ALT levels and normal liver histology.

Total RNA was isolated from mouse liver with Trizol reagent (ThermoScientific) and converted to cDNA using the High-Capacity cDNA Reverse Transcription Kit from ThermoFisher. Quantitative Reverse Transcription Polymerase Chain Reaction (qRT-PCR) was subsequently performed using the SensiFAST™ SYBR® No-ROX Kit (Bioline) following the manufacturer's instructions. Each reaction was run in triplicate to determine the threshold (CT) for each mRNA, and the amount of each cDNA relative to the β- Actin endogenous control was determined using the 2-ΔΔCt method.

2.4. Adenoviral generation of shRNA to target ASMase

Adenovirus targeting ASMase (ASMSH) was generated using the BLOCK-iT-U6 RNAi Entry Vector kit (Thermofisher) according to the manufacturer's instructions. Briefly, the kit provides a Gateway-adapted pENTRTM/U6 entry vector designed to allow efficient stable expression of shRNA targeting ASMase (top: CACCGCCTCATGAGAGCTTCTTTGGC GAACCAAACAAGCTCTCATGAGGC and bottom: AAAAGCCTCATGA-GAGCTTGTTTGGTTCGCCAAACAAGCTCTCATGAGGC) generating and cloning double stranded oligonucleotides and transforming them in

competent E.coli. Plasmid DNA was isolated with NucleoSpin Plasmid (Macherey-Nagel) and DNA sample was sent to sequence using U6 forward primer: 5′-GGACTATCATATGCTTACCG-3′ and M13 reverse primer: 5′-CAGGAAACAGCTATGAC-3'. ASMSH was transferred from the pENTRTM/U6 entry vector into the pAd/BLOCK-iTTM-DEST vector (Thermofisher) using the Gateway LR Clonase II enzyme mix. Recombinant adenoviral purified plasmid was digested with PACI and transfected into 293A cells using Lipofectamine 2000 reagent (Invitrogen). The 293A cells were maintained until 80% cytopathic effect was observed, typically 7–10 days post-transfection. Cells and media were collected and subjected to three freeze/thaw cycles. The cell debris was pelleted at 3000 rpm for 15 min, and the supernatant was used to transduce a new set of 293A cells for adenovirus amplification. Afterwards, cells were lysed and purified, and titered by plaque assay.

2.5. Primary mouse hepatocyte and mitochondria isolation

Primary mouse hepatocytes (PMH) from C57BL/6J (8 weeks old) were isolated by collagenase perfusion with flow rate of 8.5 mL/min and were cultured at a density of 0.8 × 106 cells on 60 mm dishes coated with rat tail collagen. PMH were incubated for 48 h with SAM (1 mM), SAH (0.2–5 mM) and/or Hcy (5–10 mM) at different ratios as previously described [31]. Afterwards, PMH were lysed (20 mM Tris, 0.1% Triton X-100, pH 7.0), sonicated for 5 min and *ASMase* mRNA levels and activity were determined. Mouse liver mitochondria were isolated as described previously [24,25] with minor modifications. Mitochondria (1 mL) were loaded in centrifuge tubes containing 3 and 7 mL of 60% and 26% (v/v) Percoll prepared in a buffer containing 395 mM sucrose, 0.1 mM EGTA, 10 mM Hepes-KOH, pH 7.4, and spin down at 30000 g for 15 min. Mitochondrial fraction was collected and washed with isolation buffer to remove Percoll.

2.6. Hematoxylin and Eosin, oil red and sirius red staining

Formalin fixed paraffin embedded liver biopsies from the different nutritional groups were cut into 7 μm sections and stained using standard protocols with Hematoxylin and Eosin or Sirius Red for the qualitative assessment of liver injury and fibrosis, respectively. Liver tissues were immediately frozen in liquid nitrogen and stored at −80 °C. Frozen sections of 14 μm were stained with Oil Red to determine neutral fat deposition.

2.7. Real time PCR assays

RNA was isolated using TRIzol reagent (Invitrogen). For reverse transcription, 1 μg of the total RNA was converted to first-strand cDNA using a High-Capacity cDNA Archive Kit (Applied Biosystems). Quantitative real-time PCR analysis was performed using SYBR Green (Applied Biosystems) in real-time PCR system. To normalize expression data, β-Actin was used as internal control gene. Mouse primers used in the present study are summarized in the following table.

2.8. Determination of ASMase activity

ASMase was determined from mice serum fed a CD, MCD or acute-on-chronic alcohol diet using a fluorescent sphingomyelin analog (NBD-C6-sphingomyelin, Avanti Polar Lipids) as described before [22,24]. 10 μL of serum samples were incubated for 1 h at 37 °C in incubation buffer containing 10 μM NBD-C6-sphingomyelin (250 mM sodium acetate, 0.1 mM zinc sulfate, 0.1% Triton X-100, pH 5.0). Lipids were extracted, dried in a speed vacuum, and separated by TLC (chloroform, methanol, mqH_2O; 70:25:4, v/v). NBD-ceramide was visualized under UV light, and images were acquired using ImageQuant Las4000 (GE Healthcare) and analyzed with ImageJ software.

2.9. SAM and SAH analysis

SAM and SAH were determined from deproteinized liver extracts (w/v 1:1 with perchloric acid 0.5 M) by HPLC using a 5 μm Hypersil C18 column (Waters) as previously described [32]. The isocratic elution was carried out with 40 mM ammonium phosphate, 8 mM 1-heptasulfonic acid, 6% acetonitrile, pH 5.0 adjusted with 70% perchloric acid at a flow rate of 1.0 mL/min. The UV detector (Waters 717) was set at 254 nm. SAM and SAH in biological samples were co-chromatographed with standards and identified based in their retention time. Standards (1 mM) were dissolved in 0.5 M $HClO_4$ solution, and then diluted with 0.05 M $HClO_4$ to final concentrations.

2.10. Biochemical measurements

TG and cholesterol in liver homogenates and serum ALT, AST, ethylic alcohol and homocysteine were determined by standard procedures in the Clinical Chemistry laboratory of Hospital Clinic de Barcelona. SM from liver samples was measured with a colorimetric commercial kit (Cayman). TG, total cholesterol and SM values were corrected for protein content. Total and free liver cholesterol was determined by HPLC as previously described [3]. For free cholesterol determination, 10 mg of protein were saponified with ethanol 33%-KOH and incubate at room temperature for 30 min. 400 μL of hexane and 200 μL of distilled water were added. Appropriate aliquots of the hexane layer were dried in a speed vacuum and resuspended in 200 μL of 2-propanol. HPLC analyses were made using a Waters μBondapak C18 10-μm reversed-phase column (Waters) and the mobile phase was 2-propanol/acetonitrile (50:50, v/v) at a flow rate of 1 mL/min. GSH levels were determined by the recycling method as previously described [24].

2.11. Hydroxyproline quantification

20–50 mgs of liver samples were standardized with 6 N hydrochloric acid (1:10) in a heating block at 100 °C overnight. After the mixture had cooled, 50 μL of samples and standards (1 mg/mL dissolved in 2 N NaOH) were incubated at 120 °C for 20 min. Add to the samples and standards 450 μL T-Chloramine (0.64 g in 10 mL 50% 2-propanol and 40 mL citrate-acetate buffer, pH 6.5) and incubate at room temperature for 25 min. Hydroxyproline content was measured using an Du800

Gene	Forward primer	Reverse primer
ASMase [NM_011421]	TGGGACTCCTTTGGATGGG	CGGCGCTATGGCACTGAAT
β-Actin [NM_007393]	GACGGCCAGGTCATCACTAT	CGGATGTCAACGTCACACTT
CHOP [NM_007837]	CCACCACACCTGAAAGCAGAA	AGGTGAAAGGCAGGGACTCA
Col1A [NM_007742]	GAGCGGAGAGTACTGGATCG	GTTCGGGCTGATGTACCAGT
IL-1β [NM_008361]	GAGCTGAAAGCTCTCCACCTC	CTTTCCTTTGAGGCCCAAGGC
IL-6 [NM_031168.1]	AGTCCGGAGAGGAGACTTCA	TTGCCATTGCACAACTCTTT
MCP-1 [NM_011333]	CAGCCAGATGCAGTTAACGC	GCTGCTGGTGATCCTCTTG
TGFβ	GTCAGACATTCGGGAAGCAG	GCGTATCAGTGGGGGTCA
TNFα [NM_013693]	CTGAACTTCGGGGTGATCGGT	ACGTGGGCTACAGGCTTGTCA

spectrophotometer (Beckman) at 558 nm.

2.12. Immunofluorescence

Cryopreserved liver samples from were cut on a cryostat at 14 μm thin sections and placed on glass slides. Sections were brought to RT for 30 min, fixed in 4% paraformaldehyde for 20 min and washed with PBS. The sections were permeabilized with 0.2% Triton X-100 in blocking buffer (5% goat serum + 1% BSA in PBS) for 2 h in a dark-humid chamber. Then, slices were incubated overnight at 4 °C with primary antibodies against Mat1a (PA5115549, ThermoFisher) and ASMase (PA595730, ThermoFisher) in 1% Goat Serum. After samples were incubated O.N, slices were washing × 3 with PBS. Secondary antibodies were diluted 1:200 in 1% Goat Serum and incubated for 45 min at RT with the mix of anti-mouse Alexa fluor-488. After washing, slices were mounted with immersion oil fluorescent free with DAPI (Abcam, ab104139). Images for all samples were taken with a Leica TCS SP5 laser scanning confocal system with a 63x oil immersion objective APO CS numerical aperture 1.4 equipped with a DMI6000 inverted microscope.

2.13. Lipidomic analysis

Lipidomic profiles from C57Bl/6J, *Mat1a*$^{-/-}$ and *Mat1a*$^{-/-}$*/ASMase*$^{-/-}$ subjected to CD-diet induced NASH and treated with genetic or pharmacological inhibition of ASMase were performed using UPLC-MS (OWL Metabolomics, Parque Tecnológico de Bizkaia, Derio, Spain). The UPLC-MS based platform was used to perform optimal profiling of glycerolipids, glycerophospholipids, sterol lipids and sphingolipids. Data normalization was performed following the procedure described previously [33]. Once normalized, the dimensionality of the complex data set was reduced to enable easy visualization of any metabolic clustering of the different groups of samples. This was achieved by multivariate data analysis, including the non-supervised principal components analysis (PCA) and/or supervised orthogonal partial least-square to latent structures (OPLS) approaches.

2.14. Statistical analysis

Results were expressed as mean ± SEM. Statistical significance of mean values was assessed using Student t-test and one-way ANOVA followed by Bonferroni post-test. Statistics were performed using GraphPad Prism 6 software. $p \leq 0.05$ was defined as statistically significant.

3. Results

3.1. *Mat1a*$^{-/-}$ mice exhibit selective basal ASMase activation, which further increases in CD diet-induced NASH

Disruption of methionine metabolism is a characteristic feature of steatohepatitis and can alter not only SAM/SAH but also PC synthesis from PE via PEMT [3,4,34,35]. *Mat1a*$^{-/-}$ mice exhibit increased serum methionine concentration as well as reduced hepatic SAM and GSH levels and, unlike WT mice, are predisposed to develop NASH when fed a CD diet [12]. However, the contribution of ASMase to this outcome has not been investigated. Therefore, we measured the expression of *ASMase* in *Mat1a*$^{-/-}$ mice fed a regular chow (RD) or CD diet. Basal *ASMase* mRNA levels in *Mat1a*$^{-/-}$ mice increased compared to WT mice (Suppl Figure 1A), which paralleled the stimulation of endogenous ASMase activity in *Mat1a*$^{-/-}$ mice fed RD diet (Suppl Figure 1A). This outcome was specific for ASMase, as neutral SMase activity did not increase in *Mat1a*$^{-/-}$ mice (Suppl Figure 1B). We next focused on the stimulation of ASMase in *Mat1a*$^{-/-}$ mice in the context of NASH. The basal ASMase activity further increased in *Mat1a*$^{-/-}$ mice when fed a CD diet (Suppl Figure 1A). Moreover, while WT mice fed a CD diet for 14 days developed hepatic steatosis without evidence of NASH, CD-fed *Mat1a*$^{-/-}$ mice exhibited lower body weight gain and increased liver to body weight ratio (Suppl Figure 1C), as well as exacerbated release of ALT/AST in serum (Suppl Fig. 1D), and hepatic steatosis determined by oil red staining as well as higher triglyceride levels (Suppl Figs. 1E and F). These changes were accompanied by an upregulation of proinflammatory cytokines *Tnf-α and Ccl2* (Suppl Fig. 1G) and liver fibrosis as revealed by sirius red staining and a significant induction of fibrogenic genes *Col1a1* and *Tgf*-β (Suppl Fig. 1 E, H). Moreover, total and mitochondrial GSH levels were reduced in *Mat1a*$^{-/-}$ mice fed CD diet (Suppl Fig. 1I). These data associate the susceptibility of *Mat1a*$^{-/-}$ mice to CD-mediated NASH development with the stimulation of ASMase.

3.2. Adenovirus-mediated ASMase knockdown protects *Mat1a*$^{-/-}$ mice from CD diet-induced NASH

To evaluate the causal role of ASMase in the susceptibility of *Mat1a*$^{-/-}$ mice to CD-induced NASH, we used an adenovirus-mediated shRNA expression strategy (ASMSH) to target ASMase *in vivo*. *Mat1a*$^{-/-}$ mice were fed a CD diet for 14 days and treated with either control (CtrlSH) or ASMSH adenovirus. *Mat1a*$^{-/-}$ mice fed the CD diet treated with CtrlSH adenovirus exhibited increased ASMase activity compared to *Mat1A*$^{-/-}$ mice fed a chow regular diet (RD), and this stimulation was significantly downregulated by ASMSH treatment (Fig. 1A). While ASMSH administration did not prevent the body weight gain loss and the increase of liver to body weight ratio (Fig. 1B), treatment with ASMSH protected *Mat1a*$^{-/-}$ mice from CD-mediated liver injury with decreased release of serum AST/ALT (Fig. 1C), and reduced accumulation of liver triglycerides (Fig. 1D) and hepatic steatosis, as revealed by H&E and oil red staining (Fig. 1E and F). Moreover, sirius red staining revealed the presence of fibrosis in *Mat1a*$^{-/-}$ mice fed CD diet (Fig. 1G) that paralleled the increase of hydroxyproline levels and expression of *Col1a1* and *α−sma* (Fig. 1H). Interestingly, these signs of fibrosis caused by feeding the CD diet to *Mat1a*$^{-/-}$ mice were markedly attenuated by ASMSH treatment (Fig. 1G and H). In addition, the increase in the expression of inflammatory cytokines *Tnf-α*, *Ccl2* and *Il-1β* in *Mat1a*$^{-/-}$ mice fed CD diet was significantly reduced following ASMSH administration (Fig. 1I). Thus, these findings suggest that ASMase contributes to the susceptibility of *Mat1a*$^{-/-}$ mice to CD-mediated NASH.

3.3. Pharmacological inhibition of ASMase ameliorates CD-mediated NASH development in *Mat1a*$^{-/-}$ mice

To further study the beneficial effect of genetic ASMase knockdown in the protection of *Mat1a*$^{-/-}$ mice against CD-induced NASH, we next tested whether pharmacological targeting of ASMase by amitriptyline, which has been shown to protect against diet-induced NASH [24,25,28], protects *Mat1a*$^{-/-}$ mice against CD-induced NASH. *Mat1a*$^{-/-}$ mice were fed a CD diet for 14 days with or without amitriptyline treatment (i.p. 5 mg/kg/day). As seen, amitriptyline administration significantly reduced ASMase activity in CD diet fed *Mat1a*$^{-/-}$ mice (Fig. 2A). The change in body weight and the increased liver to body weight ratio of *Mat1a*$^{-/-}$ mice fed CD was not prevented by amitriptyline (Fig. 2B), but it did protect *Mat1a*$^{-/-}$ mice from CD-induced liver injury with decreased serum ALT/AST release (Fig. 2C). Amitriptyline reduced hepatic steatosis as revealed by H&E and oil red staining (Fig. 2D and E). Moreover, amitriptyline treatment attenuated sirius red staining, and the expression of *Col1a1* and hydroxyproline levels, underscoring the ability of amitriptyline to reduce liver fibrosis in *Mat1a*$^{-/-}$ mice fed CD diet (Fig. 2F and G). Furthermore, amitriptyline administration abrogated the inflammatory response of *Mat1a*$^{-/-}$ mice fed the CD diet as seen by the reduced expression of inflammatory cytokines *Tnfα*, *Ccl2*, and *Il-1β* (Fig. 2H). Thus, collectively these finding indicate that the pharmacological inhibition of ASMase by amitriptyline is effective in protecting *Mat1a*$^{-/-}$ mice against CD-mediated NASH development.

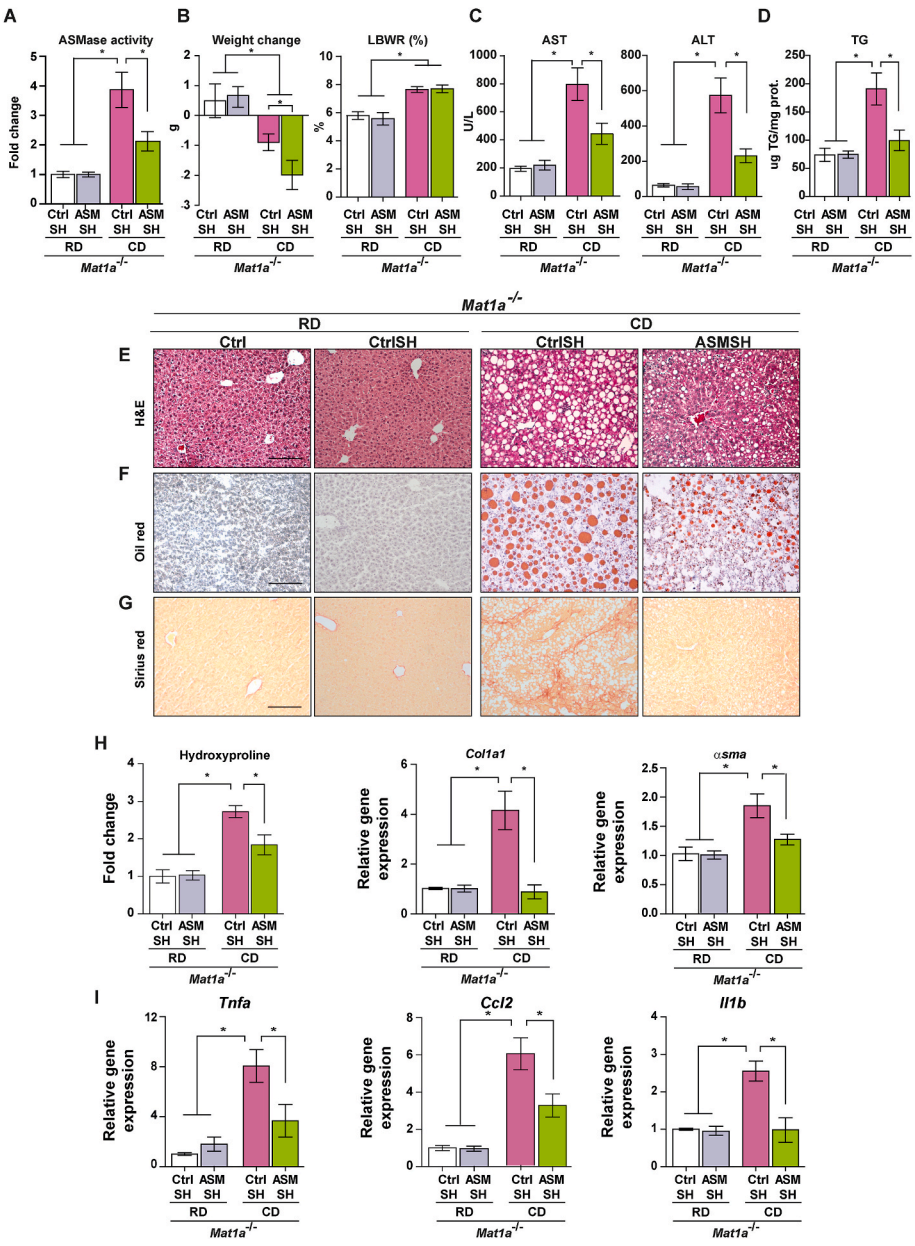

Fig. 1. ASMase knockdown protects *Mat1a*$^{-/-}$ mice against CD diet induced NASH. A, ASMase activity in *Mat1a*$^{-/-}$ mice fed RD or CD diet for 14 days with or without treatment with control SH and ASMSH adenovirus. B, Body weight and liver to body weight change in *Mat1a*$^{-/-}$ mice fed RD or CD diet for 14 days with or without treatment with control SH and ASMSH adenovirus. C, serum ALT and AST in *Mat1a*$^{-/-}$ mice fed RD or CD diet for 14 days with or without treatment with control SH and ASMSH adenovirus. D, liver triglyceride content *Mat1a*$^{-/-}$ mice fed RD or CD diet for 14 days with or without treatment with control SH and ASMSH adenovirus. E-F, representative images of H&E, and oil red staining of liver sections. G Sirius red staining of liver samples from *Mat1a*$^{-/-}$ mice fed RD or CD diet for 14 days with or without treatment with control SH and ASMSH adenovirus, with the percentage of stained areas being 2.5 ± 0.3; 3.0 ± 0.4; 12.5 ± 1.7 and 2.8 ± 0.3, respectively. H, Liver hydroxyproline content and *col1a1* and α-*sma* mRNA levels from *Mat1a*$^{-/-}$ mice fed RD or CD diet for 14 days with or without treatment with control SH and ASMSH adenovirus. I, *Tnfa*, *Ccl2* and *Il1b* mRNA levels of *Mat1a*$^{-/-}$ mice fed RD or CD diet for 14 days with or without treatment with control SH and ASMSH adenovirus. Results are mean ± SEM of N = 5–7 mice per group. *p < 0.05 *Mat1a*$^{-/-}$ mice fed CD diet treated with control SH vs ASMSH treatment. . (For interpretation of the references to color in this figure legend, the reader is referred to the Web version of this article.)

3.4. Double Mat1a/ASMase knockout mice exhibit Niemann-Pick type A disease phenotype but are protected against CD diet-induced NASH

To further explore the contribution of ASMase activation in the susceptibility of *Mat1a* knockout mice to diet-induced NASH, we crossed *Mat1a*$^{-/-}$ mice with *ASMase*$^{-/-}$ mice to generate double *Mat1a/ASMase* knockout mice. PCR, Western blot and immunofluorescence analyses revealed the deletion of both *Mat1a* and *ASMase* in the double knockout mice compared to their littermates (Supp Fig 2). As the lack of ASMase causes Niemann-Pick type A (NPA) disease [21,29], a lysosomal storage disorder characterized by increased lipid accumulation in brain and visceral organs (e.g. liver) and neurological deficits, double *Mat1a/-ASMase* knockout mice exhibited abnormal growth, cachexia, ataxia and trembling. Double *Mat1a/ASMase* knockout mice at 6 weeks of age exhibited increased hepatic SM levels characteristic of NPA disease, and basal elevation of Tnf-α without evidence of overt alterations in liver histology and basal injury (Suppl Figs. 3A–D). We next addressed the susceptibility of double *Mat1a/ASMase* knockout mice to diet-induced NASH. Given the impact of ASMase deletion in the progressive deterioration of motor coordination, *Mat1a/ASMase* double knockout mice were fed a CD diet for 7 days. ASMase activity increased in *Mat1a*$^{-/-}$ mice fed CD diet that was completely abolished in the double *Mat1a/ASMase* knockout mice (Fig. 3A). ASMase deletion in *Mat1a*$^{-/-}$ mice did not significantly affect body weight loss or the increased liver to body weight ratio following administration of the CD diet (Fig. 3A). H&E analyses of *Mat1a*$^{-/-}$ mice fed the CD diet for 7 days revealed the presence of macrovesicular steatosis as revealed by oil red staining, and these effects were markedly attenuated in the double *Mat1a/ASMase* knockout mice fed CD diet (Fig. 3B and C), in line with the reduced liver triglyceride content (Fig. 3D). Moreover, sirius red staining indicated the onset of liver fibrosis in *Mat1a*$^{-/-}$ mice fed CD diet, and this outcome was reduced in the double *Mat1a/ASMase* knockout mice (Fig. 3E) that paralleled the decrease in hydroxyproline levels (Fig. 3F) and expression of *Col1a and Pdgfr* (Fig. 3G). In addition, feeding the CD diet for 7 days to *Mat1a*$^{-/-}$ mice resulted in inflammation with increased expression of *Ccl2* and *Il-1β* that was attenuated in the double *Mat1a/ASMase* knockout mice (Fig. 3H). Thus, these findings underscored that the genetic ablation of ASMase protected *Mat1a*$^{-/-}$ mice against diet-induced

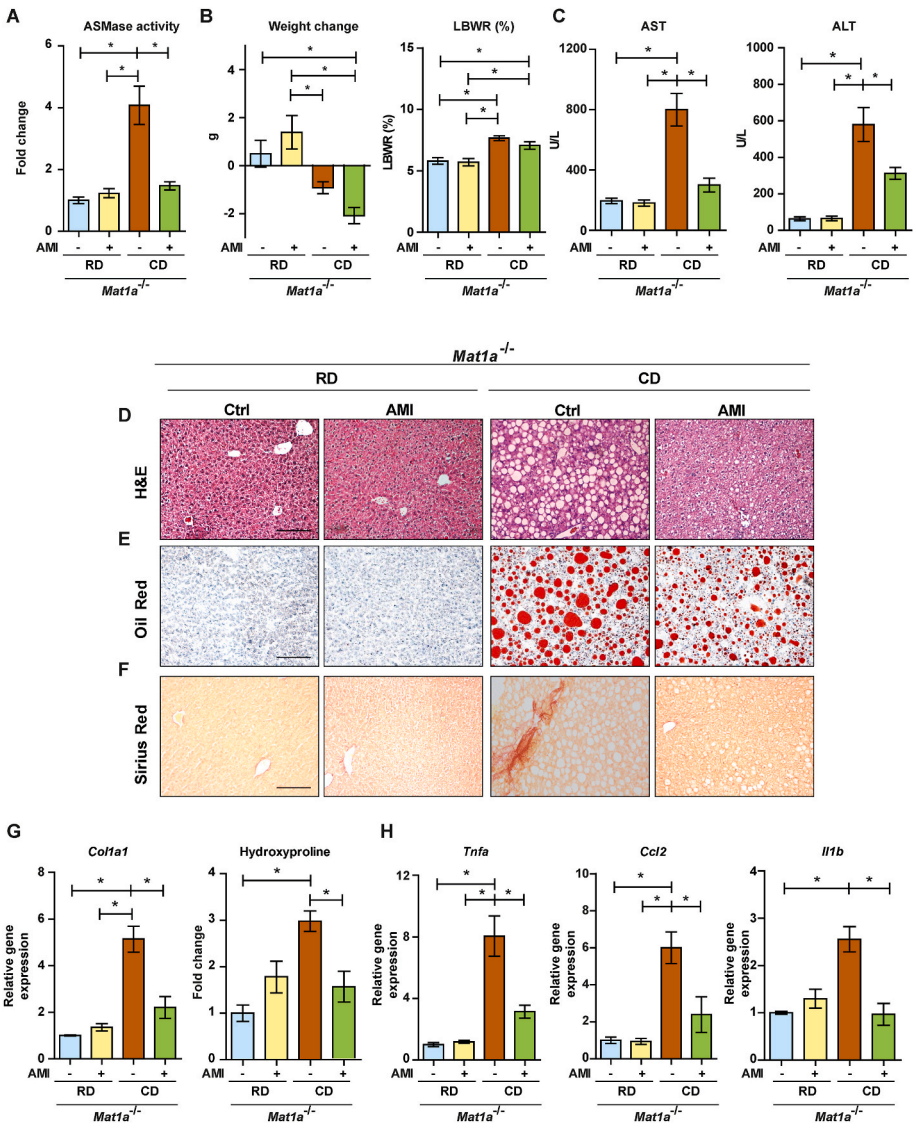

Fig. 2. Pharmacological ASMase inhibition protects *Mat1a*$^{-/-}$ mice against CD diet induced NASH. A, ASMase activity in *Mat1a*$^{-/-}$ mice fed RD or CD diet for 14 days with or without amitriptyline (AMI) treatment to block ASMase. B, Body weight and liver to body weight change in *Mat1a*$^{-/-}$ mice fed RD or CD diet for 14 days with or without AMI. C, serum ALT and AST of *Mat1a*$^{-/-}$ mice fed RD or CD diet for 14 days with or without AMI treatment. D-E, representative images of H&E and oil red staining of liver sections. F, Sirius red staining of liver samples from *Mat1a*$^{-/-}$ mice fed RD or CD diet for 14 days with or without AMI treatment, with the percentage of stained areas being 2.6 ± 0.4; 3.2 ± 0.5; 18.4 ± 2.1 and 4.1 ± 0.5, respectively. G, *Col1a1* mRNA levels and liver hydroxyproline from *Mat1a*$^{-/-}$ mice fed RD or CD diet for 14 days with or without AMI treatment. H, *Tnfa*, *Ccl2* and *Il1b* mRNA levels of *Mat1a*$^{-/-}$ mice fed RD or CD diet for 14 days with or without AMI treatment. Results are mean ± SEM of N = 5–7 mice per group. *p < 0.05 *Mat1a*$^{-/-}$ mice fed CD diet treated with AMI vs control. . (For interpretation of the references to color in this figure legend, the reader is referred to the Web version of this article.)

NASH.

3.5. Amitriptyline treatment protects WT mice from MCD diet-induced NASH

Despite its impact in the net loss of body weight, feeding a methionine and choline deficient (MCD) diet is a common nutritional model of NASH that it is characterized by liver injury with elevated serum transaminases levels, steatosis, inflammation, and fibrosis [36]. Although both methionine and choline are deficient in the MCD diet, the specific lack of methionine is responsible for most of the deleterious effects of the MCD diet [26]. Except for the dissociation from obesity and the loss of body weight, histological changes observed in mice fed MCD are similar to those observed in human NASH [36]. Hence, we anticipated that feeding WT mice the MCD diet would be equivalent to feeding *Mat1a*$^{-/-}$ mice the CD diet, and therefore we tested the role of inhibition of ASMase in the MCD NASH model. WT mice were fed a MCD diet for 14 days with or without amitriptyline treatment. Consistent with the observations in *Mat1a*$^{-/-}$ mice fed a CD diet, amitriptyline treatment in WT mice ameliorated the increase in ASMase activity induced by MCD feeding, although it did not reverse the liver to body weight loss (Fig. 4A). This outcome translated in a significant protection against MCD-induced liver injury as seen by the decrease in the release of serum ALT/AST (Fig. 4B). Moreover, amitriptyline administration reduced hepatic steatosis and the increase in triglyceride content in WT mice fed MCD diet (Fig. 4C, D, E). In addition, MCD feeding induced liver fibrosis in WT mice and this effect was prevented by amitriptyline treatment (Fig. 4F) that paralleled the decrease of hydroxyproline levels and reduced expression of *α-sma* (Fig. 4G). Furthermore, feeding the MCD diet induced inflammation in WT mice, as reflected by the increased expression of the inflammatory cytokines *Ccl2* and *Il-1β* that was attenuated upon amitriptyline administration (Fig. 4H). Thus, these data underscore that feeding WT mice a MCD diet phenocopies the susceptibility of *Mat1a*$^{-/-}$ mice to develop NASH when fed a CD diet and that in both cases the pharmacological inhibition of ASMase is protective.

3.6. ASMase contributes to the alterations of the liver lipidome of *Mat1a*$^{-/-}$ mice

As changes in molecular lipid signatures determine different subtypes of NASH [37], we next examined the contribution of ASMase in the lipidome profile of *Mat1a*$^{-/-}$ mice fed CD diet with or without genetic and pharmacological targeting of ASMase. A total of 266 metabolites were detected in the liver samples of mice with different genetic backgrounds fed the CD diet with or without adenoviral or pharmacological ASMase inhibition and were subjected to univariate data analyses

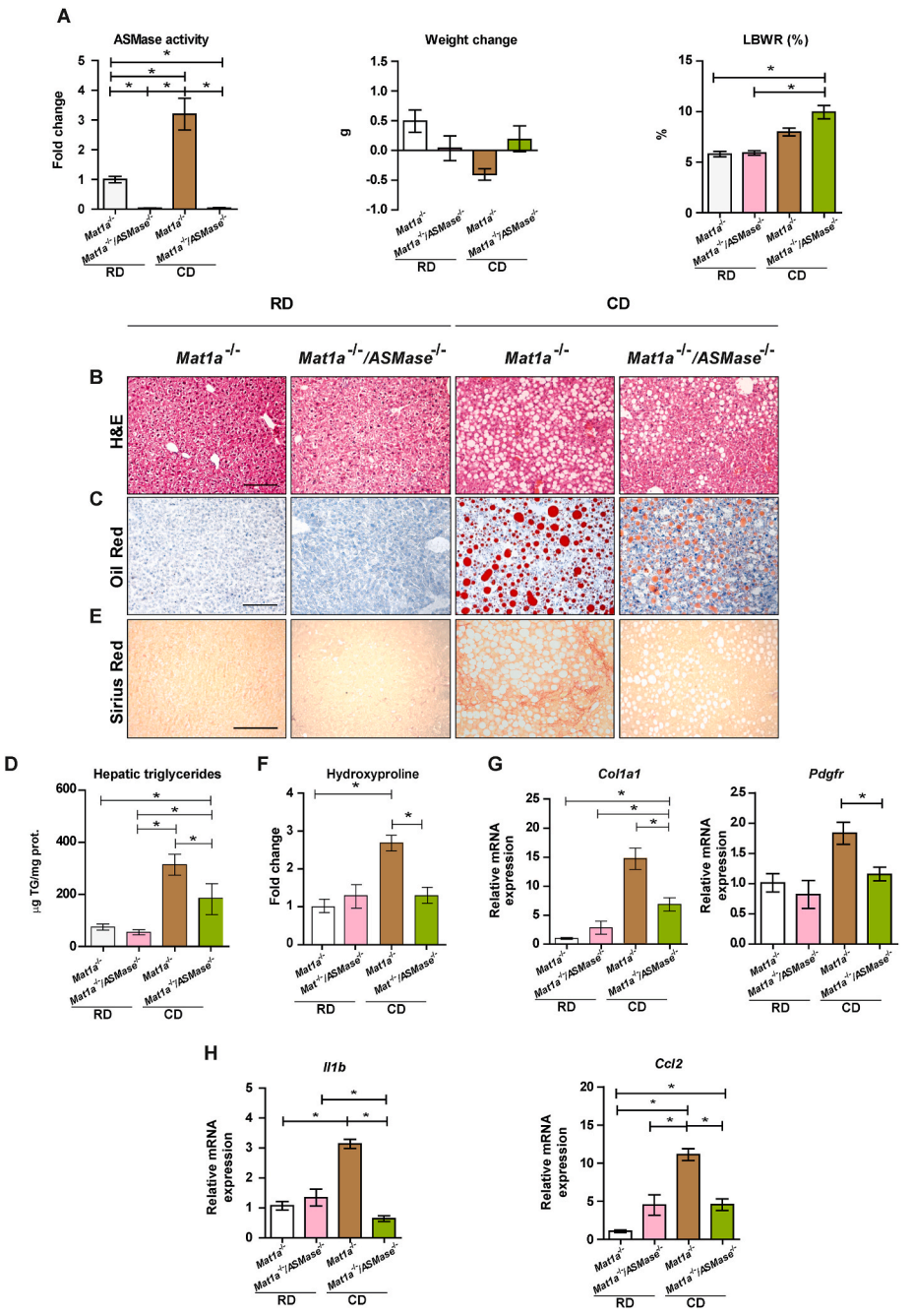

Fig. 3. *Mat1a*$^{-/-}$*/ASMase*$^{-/-}$ double knockout mice are protected against CD diet induced NASH. A, ASMase activity and body weight and liver to body weight changes from *Mat1a*$^{-/-}$ and *Mat1a*$^{-/-}$*/ASMase*$^{-/-}$ mice fed RD or CD diet for 7 days. B–C, H&E and oil red staining of liver samples from *Mat1a*$^{-/-}$ and *Mat1a*$^{-/-}$*/ASMase*$^{-/-}$ mice fed RD or CD diet for 7 days. D, liver triglycerides levels from *Mat1a*$^{-/-}$ and *Mat1a*$^{-/-}$*/ASMase*$^{-/-}$ mice fed RD or CD diet for 7 days. E, Sirius red staining of liver samples from *Mat1a*$^{-/-}$ and *Mat1a*$^{-/-}$*/ASMase*$^{-/-}$ mice fed RD or CD diet for 7 days, with the percentage of stained areas being 2.8 ± 0.4; 3.1 ± 0.4; 13.6 ± 1.6 and 3.5 ± 0.4, respectively. F, Liver hydroxyproline levels from *Mat1a*$^{-/-}$ and *Mat1a*$^{-/-}$*/ASMase*$^{-/-}$ mice fed RD or CD diet for 7 days. G, *Col1a1* and *Pdgfr* mRNA levels of liver samples from *Mat1a*$^{-/-}$*/ASMase*$^{-/-}$ mice fed RD or CD diet for 7 days. H, *Il1b* and *Ccl2* mRNA levels of liver samples from *Mat1a*$^{-/-}$*/ASMase*$^{-/-}$ mice fed RD or CD diet for 7 days. Results are mean ± SEM of N = 5–7 mice per group. *p < 0.05 *Mat1a*$^{-/-}$*/ASMase*$^{-/-}$ mice vs. *Mat1a*$^{-/-}$ fed CD diet. . (For interpretation of the references to color in this figure legend, the reader is referred to the Web version of this article.)

(Fig. 5). A heatmap of the genetic background revealed differences between livers of double *Mat1a/ASMase* knockout mice compared to *Mat1a*$^{-/-}$ and WT mice fed regular diet (Fig. 5A). For instance, while a similar lipidomic profile between *Mat1a*$^{-/-}$ mice and WT mice fed regular diet was observed glycerolipids, especially all the DAG and TAG, and particularly SM and cholesterol in the double *Mat1a/ASMase* knockout mice increased compared to WT and *MAT1a*$^{-/-}$ mice fed regular diet (Fig. 5A), likely reflecting the phenotype of NPA due to the lack of ASMase.

Moreover, univariate data analyses revealed that feeding CD diet to *Mat1a*$^{-/-}$ mice induced more pronounced changes in lipid species than in CD-fed WT mice, with a significant increase in glycerolipids TAG, DAG and MAG, sterol lipids ChoE and glycerophospholipids (MEMAPC and MEMAPE), while DAPC, DAPE and PI decreased (Fig. 5B). However, the changes observed in double *Mat1a/ASMase* knockout mice fed CD diet were less significant, exhibiting a similar lipidomic profile as double *Mat1a/ASMase* knockout mice fed regular diet (Fig. 5B). The increase in glycerolipids and glycerophospholipids species observed in *Mat1a*$^{-/-}$ mice or double *Mat1a/ASMase* fed CD diet were similar to WT mice fed CD diet, while sphingolipids increased in double *Mat1a/ASMase* mice fed CD diet compared to *Mat1a*$^{-/-}$ mice fed CD diet (Fig. 5B). Similar changes in the lipidomic profile of *Mat1a*$^{-/-}$ fed CD diet was observed when ASMase was targeted genetically by ASMSH or inhibited pharmacologically with amitriptyline (Fig. 5C), indicating that antagonizing ASMase abrogates the changes in the lipidomic profile of *Mat1a*$^{-/-}$ induced by CD diet feeding. Thus, although germline deletion of ASMase in *Mat1a*$^{-/-}$ induces an endogenous basal steatosis reflecting the liver manifestation of the NPA disease, ASMase antagonism prevents most of the alterations in the lipidome profile of *Mat1a*$^{-/-}$ caused by the CD diet.

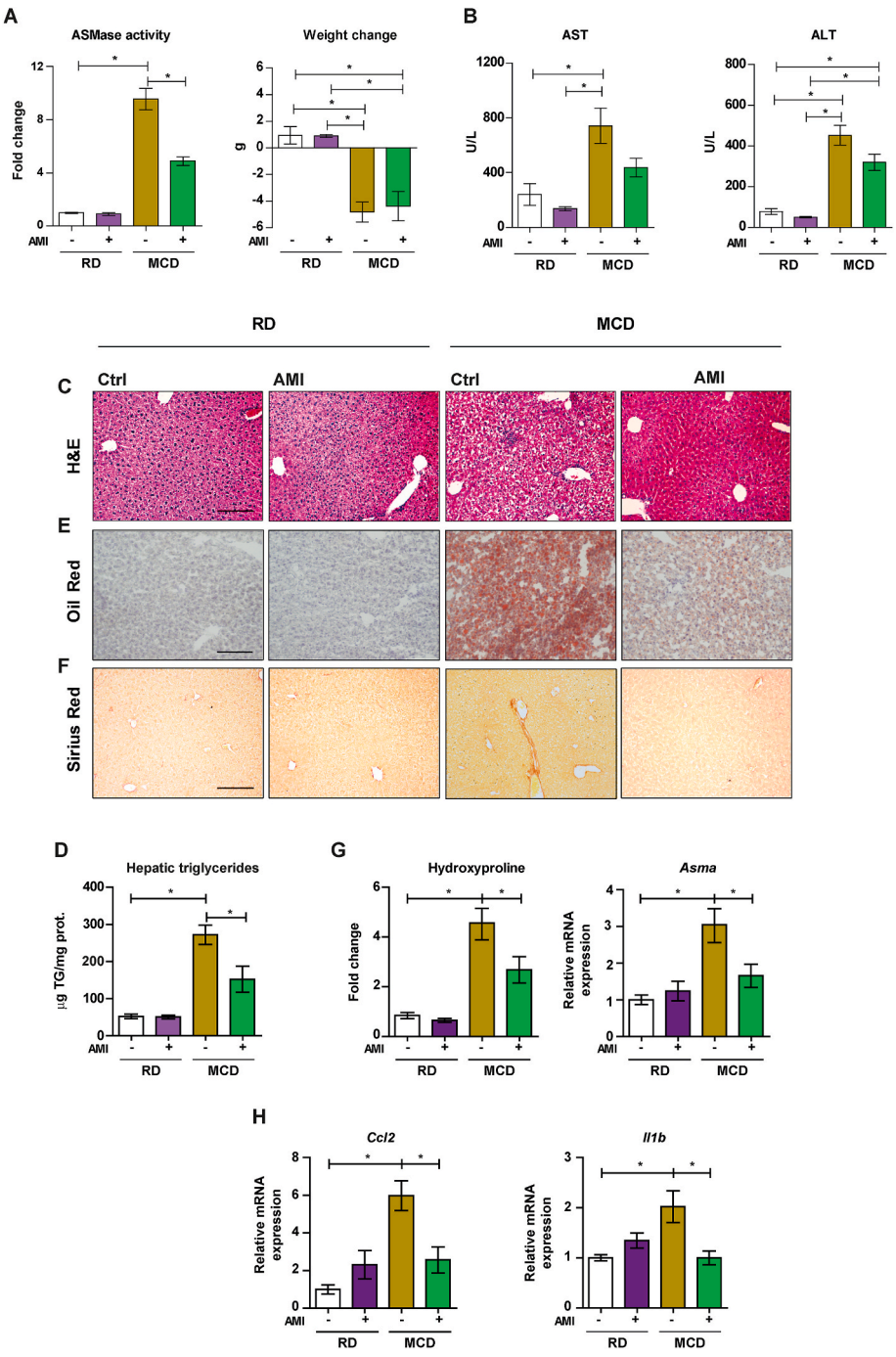

Fig. 4. Amitriptyline of ASMase protects WT mice against MCD-induced NASH. A, ASMase activity and body weight change of WT mice fed RD or MCD for 14 days with or without amitriptyline (AMI) treatment. B, serum ALT and AST of WT mice fed RD or CD diet for 14 days with or without AMI treatment. C, H&E, oil red and Sirius red staining of liver samples from WT mice fed RD or CD diet for 14 days with or without AMI treatment. D, Hepatic triglyceride content of WT mice fed RD or CD diet for 14 days with or without AMI treatment. E-F, Oil red and Sirius red staining of liver samples from WT mice fed RD or CD diet for 14 days with or without AMI treatment, with the percentage of stained areas being 2.5 ± 0.3; 2.7 ± 0.3; 15.2 ± 1.57 and 2.9 ± 0.4, respectively. G, Hydroxyproline and α-*sma* mRNA levels of WT mice fed RD or CD diet for 14 days with or without AMI treatment. H, *Ccl2* and *Il1b* mRNA of WT mice fed RD or CD diet for 14 days with or without AMI treatment. Results are mean ± SEM of N = 5–7 mice per group. *p < 0.05 WT mice fed MCD diet vs. AMI and WT *mice* fed CD diet. . (For interpretation of the references to color in this figure legend, the reader is referred to the Web version of this article.)

3.7. ASMase contributes to the susceptibility of *Mat1a*$^{-/-}$ mice to ASH

Given the contribution of ASMase to the susceptibility of *Mat1a*$^{-/-}$ mice to nutritional NASH, we next examined whether *MAT1A* deletion predisposes to ASH and the role of ASMase. We used the well-characterized NIAAA acute-on-chronic model of alcohol-related liver disease [30]. Compared to WT mice, *Mat1a*$^{-/-}$ mice subjected to this approach of alcohol feeding exhibited a further stimulation of ASMase activity (Suppl Fig. 4A). Moreover, while this pattern of alcohol feeding induced CYP2E1 and serum alcohol levels in WT and *Mat1a*$^{-/-}$ mice to a similar extent (Suppl Figs. 4B and C), the degree of liver injury, hepatic steatosis and the increase in liver triglycerides were more pronounced in *Mat1a*$^{-/-}$ mice than in WT mice (Suppl Fig. 4 D-F). Sirius red staining indicated the onset of liver fibrosis in *Mat1a*$^{-/-}$ mice fed alcohol compared to WT mice (Suppl Fig. 4G).

We next assessed the contribution of ASMase to the susceptibility of *Mat1a*$^{-/-}$ mice to ASH by adenovirus-mediated shRNA expression targeting ASMase (ASMSH). ASMSH significantly decreased the stimulation of ASMase caused by acute-on-chronic alcohol feeding (Fig. 6A). In addition, ASMSH treatment diminished acute-on-chronic alcohol induced release of serum ALT/AST (Fig. 6B) and hepatic steatosis in *Mat1a*$^{-/-}$ mice as revealed by H&E and oil-red and sirius red staining (Fig. 6C and D), without affecting serum alcohol levels (Fig. 6F). Moreover, Sirius red staining (Fig. 6E) indicated a protective effect of

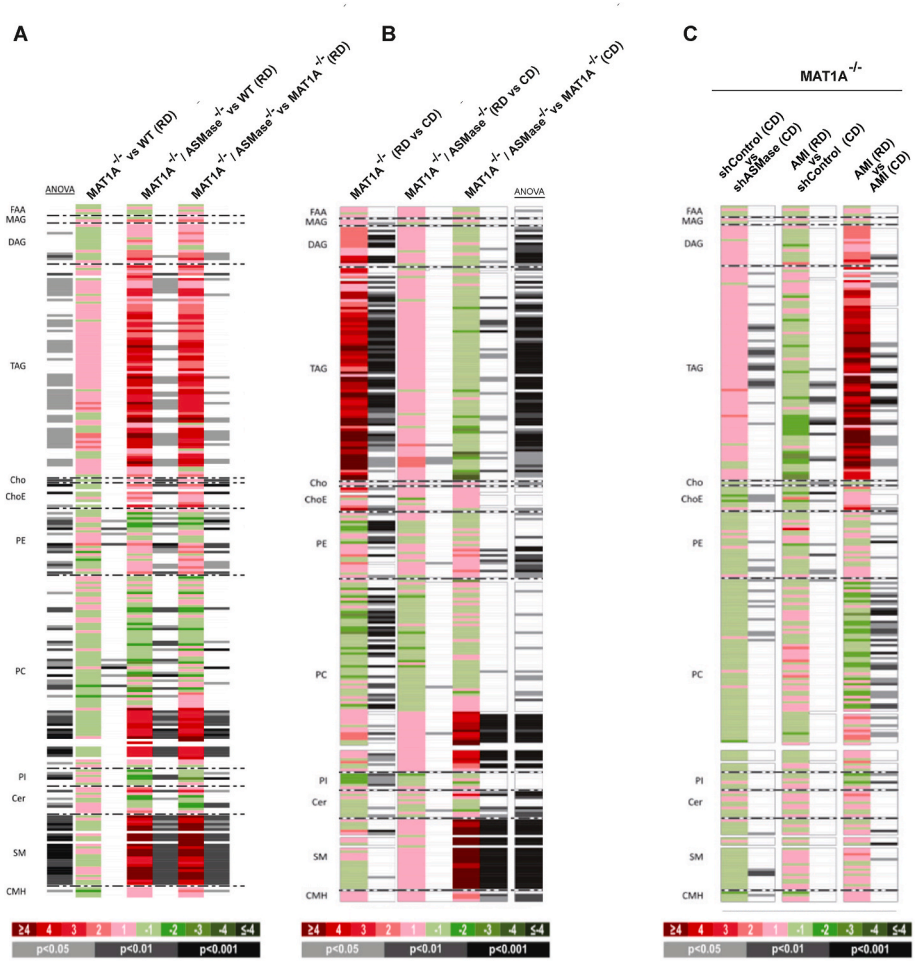

Fig. 5. Heatmap of lipidome profile of WT, *Mat1a*$^{-/-}$ and *Mat1a*$^{-/-}$*/ASMase* mice fed RD and CD diet. A-C, Heatmap representing individual lipidomic classes obtained from the comparison of the genetic background of mice (A), diet RD vs CD (B) and treatment to target ASMase (C). Color codes are presented as log2 (fold-change) and paired Student's *t*-test p-values indicated at the bottom of figure. N = 5 mice per group and comparison were used for the lipidomic analyses. . (For interpretation of the references to color in this figure legend, the reader is referred to the Web version of this article.)

ASMSH in the development of liver fibrosis of *Mat1a*$^{-/-}$ mice that was confirmed by the downregulation of *Col1A1*, *Tgf-β* and hydroxyproline levels (Fig. 6G). Furthermore, the acute-on-chronic alcohol-induced expression of inflammatory cytokines *Tnfα*, *Ccl2* and *Il-6* in *Mat1a*$^{-/-}$ mice was attenuated by ASMSH treatment (Fig. 6H). Collectively, these findings underscore that deletion of *MAT1A* sensitizes to ASH by the stimulation of ASMase.

3.8. Low SAM/SAH ratio induces ASMase expression

Since *MAT1A* deletion induces the endogenous expression of ASMase, we next investigated the potential mechanism underlying this effect. Consistent with the key role of MATI/III in the synthesis of SAM from methionine, *Mat1a*$^{-/-}$ mice exhibit substantial depletion of hepatic SAM and increased SAH levels [12]. Therefore, we tested the impact of increasing SAH and homocysteine (Hcy) concentrations on the regulation of ASMase expression. Primary mouse hepatocytes (PMH) were isolated and incubated with different concentrations of SAM and SAH to establish different SAM/SAH ratios, which cause oxidative and ER stress [31,32,38]. As seen, while incubation with 1 mM SAM or 0.2 mM SAH did not affect ASMase expression, exposure of PMH to 5 mM SAH significantly increased the mRNA level of *ASMase* similar to the stimulation observed upon incubation of PMH with a SAM/SAH of 0.2 (Fig. 7A), which translated in a significant increase in ASMase activity (Fig. 7B). In line with these findings, incubation with increasing concentrations of Hcy resulted in the stimulation of *ASMase* expression (Fig. 7A). Thus, these findings indicate that decreased SAM/SAH ratio stimulates the expression of *ASMase*.

3.9. Inversed relationship between MAT1A and ASMase expression in human ASH and NASH

Consistent with the susceptibility of *Mat1a*$^{-/-}$ mice to develop NASH, previous findings have shown that patients with NASH and alcoholic cirrhosis exhibit down regulation of *MAT1A* expression and low SAM levels [39–42]. Moreover, increased expression of *ASMase* has been reported in patients with ASH and NASH [24,25]. However, the relationship and expression of MAT1A and ASMase in the same cohort of patients with ASH and NASH have not been determined. Therefore, we next examined the expression of both MAT1A and ASMase in liver samples from patients with ASH and NASH. In line with previous findings, *MAT1A* mRNA levels were reduced in samples from both ASH and NASH, while those of *ASMase* increased (Fig. 8A and B). In addition, an inversed correlation between the expression of MAT1A and ASMase was observed in the cohort of patients with ASH and NASH (Fig. 8C–E). These findings along with the reported downregulation of MAT1A by ASMase [27], suggest that MAT1A deletion and ASMase activation engage in a self-sustained loop, which may be of relevance to human ASH and NASH.

4. Discussion

Disruption of methionine metabolism, illustrated by the decreased expression and activity of MAT1A, and the induction of ASMase are known to individually promote NASH. However, whether these players are functionally interrelated and work in concert to favor the transition from steatosis to NASH has not been previously addressed. Although first described in the context of fulminant liver failure that ASMase

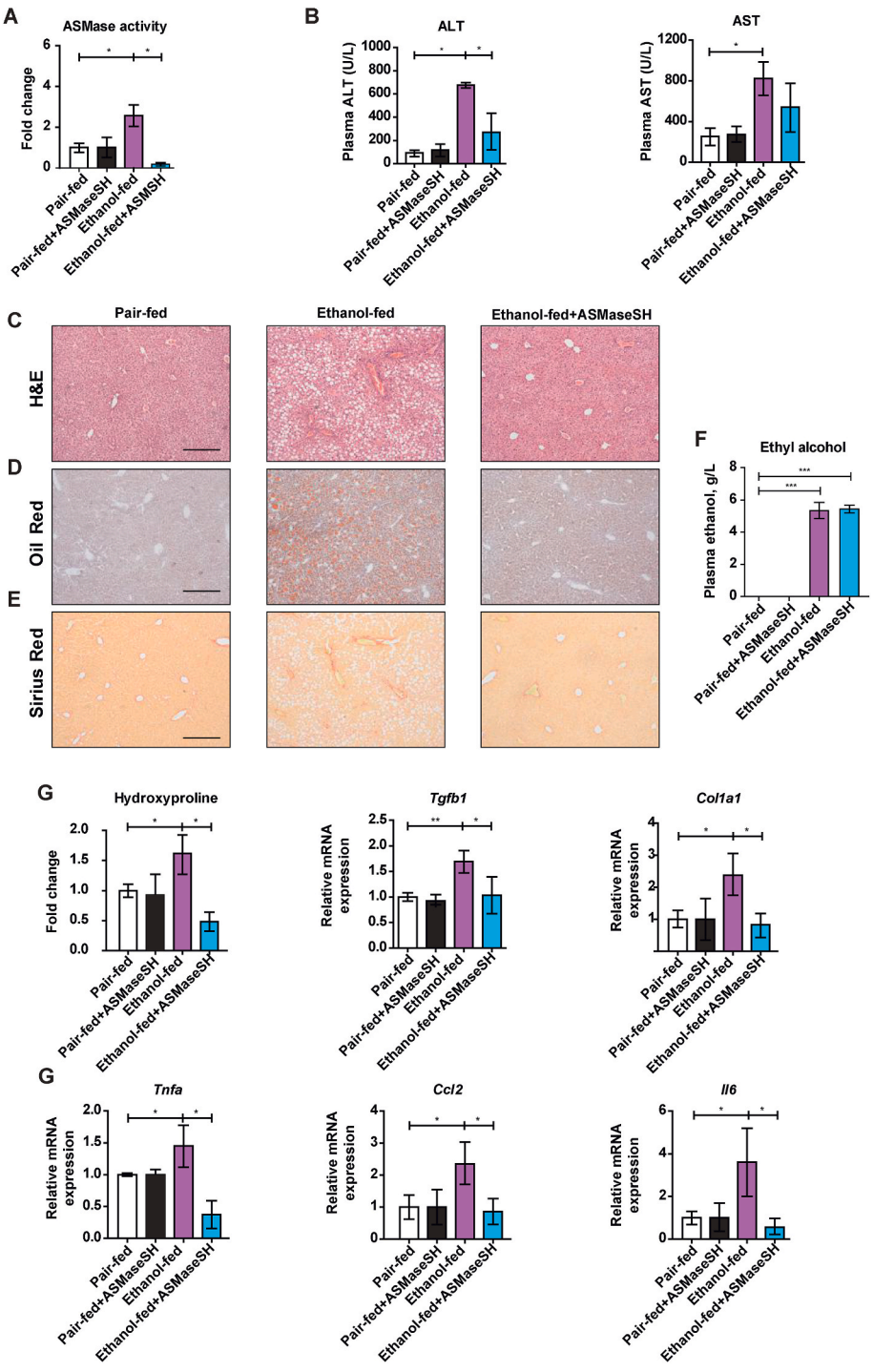

Fig. 6. ASMase knockdown protects *Mat1a*$^{-/-}$ mice against alcohol induced liver disease. A, ASMase activity from *Mat1a*$^{-/-}$ mice fed acute-on-chronic alcohol with or without treatment with control SH and ASMSH adenovirus. B, serum ALT and AST of *Mat1a*$^{-/-}$ mice fed acute-on-chronic alcohol with or without treatment with control SH and ASMSH adenovirus. C-D, representative images of H&E and Oil red staining of liver sections. F, Sirius red staining for liver samples from *Mat1a*$^{-/-}$ mice fed acute-on-chronic alcohol with or without treatment with control SH and ASMSH adenovirus, with the percentage of stained areas being 2.4 ± 0.3; 12.1 ± 1.4 and 2.5 ± 0.3, respectively. F, serum ethanol levels of *Mat1a*$^{-/-}$ mice fed acute-on-chronic alcohol with or without treatment with control SH and ASMSH adenovirus. G, Hepatic hydroxyproline levels and *Tfgb* and *Col1a*1 mRNA levels of *Mat1a*$^{-/-}$ mice fed acute-on-chronic alcohol with or without treatment with control SH and ASMSH adenovirus. H, *Tnfa*, *Ccl2* and Il6 mRNA levels from *Mat1a*$^{-/-}$ mice fed acute-on-chronic alcohol with or without treatment with control SH and ASMSH adenovirus. Results are mean ± SEM of N = 5–7 mice per group. *p < 0.05 vs. *Mat1a*$^{-/-}$ mice fed pair-fed diet or ethanol diet plus ASMSH treatment. . (For interpretation of the references to color in this figure legend, the reader is referred to the Web version of this article.)

regulates MAT1A mRNA stability [27], in this study, we extend these observations and show that decreased MAT1A expression induces the stimulation of ASMase, suggesting a reciprocal regulation in which MAT1A and ASMase engage in a self-amplified circle, which sustains NASH progression. We use both dietary and genetic models of disruption of methionine metabolism, in which a common element of these disparate approaches is the decrease in SAM levels, a key intermediate metabolite synthesized from methionine by MAT1A. Mice with global *Mat1a* deletion has been an instrumental model that not only demonstrates the crucial role of SAM in liver biology and metabolism [12], but it is used as a golden standard to validate the lipidomic findings reported in patients with NASH [37]. Both WT mice fed a MCD diet or *Mat1a* knockout mice fed a CD diet exhibit decreased SAM/SAH, which directly induced the expression of ASMase, as shown in the *in vitro* PMH studies in the current study. Although previous findings in the context of NPA disease linked the methylation status of the *SMPD1* promoter with ASMase expression [43], it remains to be established whether the decreased SAM/SAH ratio and high Hcy causing enhanced ASMase induction is directly related to the methylation state of the SMPD1 promoter in CpG sites, underlying a potential epigenetic regulation of ASMase. Alternatively, high Hcy has been shown to induce ER stress [38], leading to the hypothesis that ER stress may stand as a potential regulator of ASMase expression. This possibility implies that ER stress and ASMase engage in a self-promoting circle, as ASMase is required for

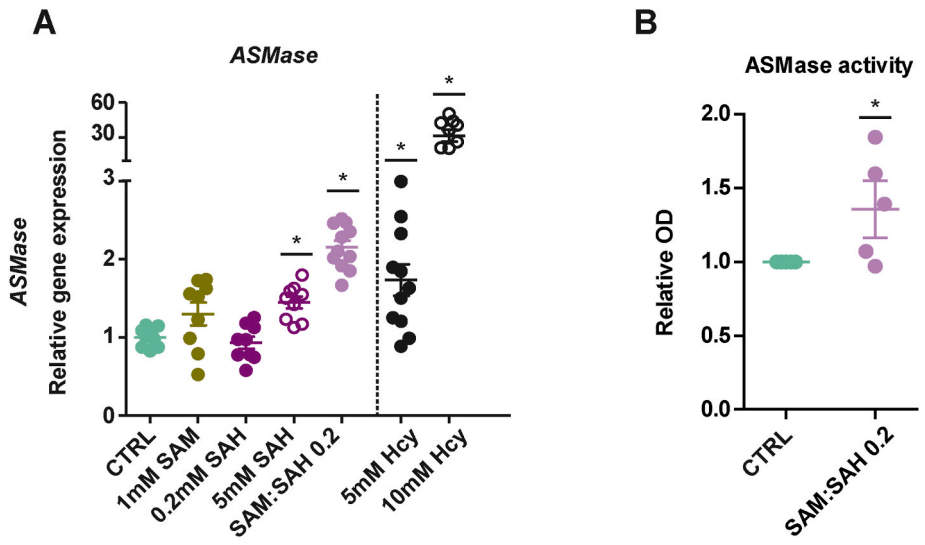

Fig. 7. Low SAM/SAH and increased HCY induce the expression of ASMase.Primary isolated hepatocytes were isolated and incubated with SAM (1 mM), SAH (0.2–5 mM) and homocysteine (5–10 mM) as indicated. Cells extracts were used for the determination of ASMase mRNA levels and activity as described in Methods. Results are mean ± SEM of N = 5–12 PMH preparations. *p < 0.05 vs. control PMH.

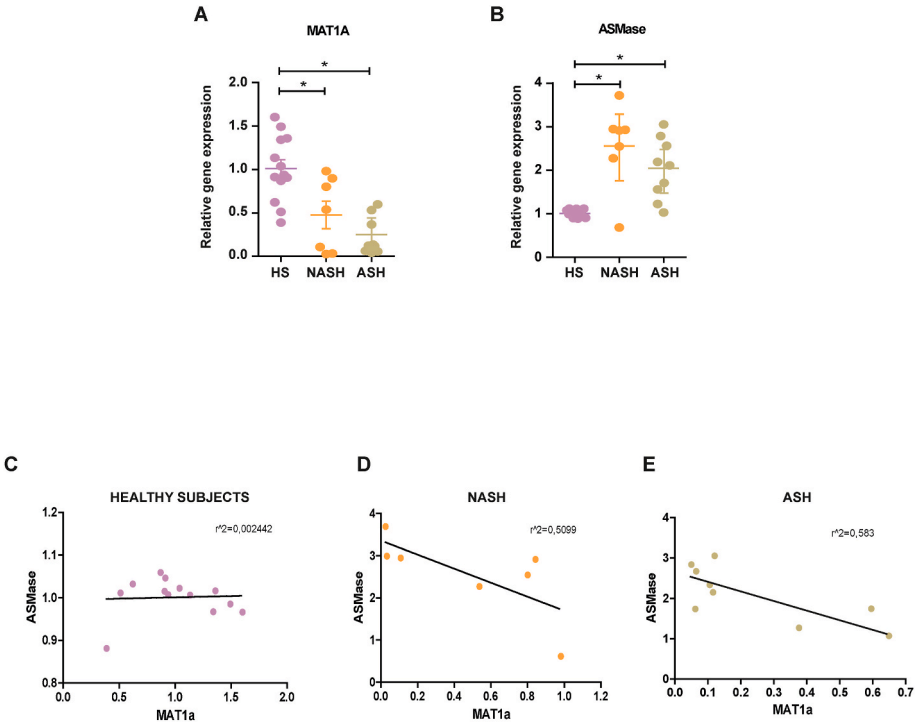

Fig. 8. MAT1A and ASMase mRNA levels from liver samples of patients with ASH and NASH. A-B, Liver samples from control subjects and patients with ASH and NASH were used to determine the mRNA of MAT1A and ASMase. C-E, Correlation between the mRNA of ASMase and MAT1A in the cohort of patients with ASH and NASH. Clinical characteristics of patients are shown in Supplementary Table 1. *p < 0.05 vs. control subjects.

the onset of ER stress in the context of alcohol-related liver disease [24]. In addition, copper-induced oxidative stress has been shown to induce ASMase activity in Wilson's disease [44], and hence it is conceivable that in conditions of low SAM and high SAH that induce ASMase may involve an oxidative stress-dependent mechanism.

If one side of the coin is the repression of MAT1A by the ASMase [27], the other side is the stimulation of ASMase by decreased MAT1A expression, as shown here, which can result in two major changes in sphingolipid metabolism, including the decrease of SM in membrane bilayers and the subsequent generation of ceramide is specific sites, which underlie the deleterious effects of ASMase induction. Indeed, increased ceramide, the prototype sphingolipid, is known to regulate multiple cell functions and pathways, such as cell death, senescence, inflammation, as well as gene expression [15,16,45], and has been consistently implicated in insulin resistance and the pathogenesis of NASH [46,47]. Indeed, ASMase stimulation has been shown to shorten the half-life of *MAT1A* mRNA, an effect that is abolished by cycloheximide to prevent protein synthesis [27]. Consistent with the effect of ASMase on the stability of *MAT1A* mRNA, previous findings in Jurkat cells indicated that ceramide C2 shortened the half-life of Bcl-2 mRNA through a conserved AU-rich element in the 3′ untranslated region of Bcl-2 mRNA [48], lending further support that ASMase-induced

ceramide generation signals the posttranslational decay of MAT1A mRNA by a mechanism involving the recruitment of the exosome by AU-binding proteins to affect 3′-to-5′ mRNA degradation [49]. Although further work will be required to fully understand the underlying mechanism whereby the ceramide pool generated by ASMase regulates the stability of the *MAT1A* mRNA, the current findings indicate that the restriction of MAT1A expression and the induction of ASMase engage in a self-amplifying spiral that promotes steatohepatitis.

An important feature of the present study is that targeting ASMase protects against diet-induced NASH and ASH. In addition to the deleterious effects of ASMase-derived ceramide as a trigger of hepatocellular apoptosis and liver fibrosis [23–25], this pool of ceramide regulates lipid homeostasis and hence hepatic steatosis. In this regard, ceramide can lead to the abrogation of PC generation by at least two different and complementary mechanisms, namely through the downregulation of SAM as shown here, which can limit the synthesis of PC from the methylation of PE via PEMT [29]. Although this pathway of PC synthesis from PE accounts for a minor fraction of the total PC in cells (15–20%), ceramide can also negatively impact the *de novo* synthesis of PC from choline in the Kennedy pathway. For instance, ceramide has been shown to inhibit the CTP: phosphocholine cytidylyltransferase step in the PC arm of the Kennedy pathway, leading to increased phosphocholine level and reduced generation of PC [50,51]. Consistent with these findings, we show that targeting ASMase by genetic or pharmacological approaches decreases hepatic steatosis in *Mat1a*$^{-/-}$ mice in the context of ASH and NASH. As mitochondrial dysfunction and subsequent oxidative stress can lead to hepatic steatosis and progression towards NASH [52], further investigation will be required to establish whether the reciprocal regulation of *MAT1A* deletion and ASMase stimulation impacts mitochondrial function and elicits oxidative stress. In line with this potential link, recent findings reported that MAT1A is found in mitochondria to preserve mitochondrial function, and that its mitochondrial loss worsens ALD [53]. Whether the depletion of mitochondrial MAT1A involves stimulation of ASMase to promote steatohepatitis remains to be established. Moreover, a potential relationship between changes in lipid composition of fatty acids, especially the decrease in the levels of n-3 polyunsaturated fatty acids, which are related to oxidative stress and diet-induced NASH [54], and the self-sustained cycle between *MAT1A* deletion and ASMase stimulation deserves to be examined in future studies.

While our findings underscore a reciprocal regulation between MAT1A downregulation and ASMase activation in ASH and NASH, a remaining question to address in future studies is the elucidation of which event precedes the other and if MAT1A reduction occurs before ASMase activation in dietary ASH/NASH models. Our findings showing that dietary or genetic MAT1A downregulation activates ASMase to promote steatohepatitis is intriguing *vis-a-vis* recent observations that downregulation of *Mat1a* by antisense oligonucleotides (ASO) protects mice against diet-induced NASH [55]. Unfortunately, Saenz de Urturi et al. did not examine the impact of Mat1a ASO in the status of ASMase and further investigations will be required to establish the critical threshold of MAT1A downregulation without incurring in ASMase activation. In summary, the present study reveals a reciprocal regulation of MAT1A and ASMase, which engage in a self-amplification loop of relevance for the development of ASH and NASH.

Grant support

This project has received funding from the European Horizon's research and innovation programme HORIZON-HLTH-2022-STAYHLTH-02 under agreement No 101095679. We acknowledge the support from grants PID2019-111669RB, and PID2020-115055RB-I00 from Plan Nacional de I + D funded by the Agencia Estatal de Investigación (AEI) and the Fondo Europeo de Desarrollo Regional (FEDER) and from the CIBEREHD; the center grant P50AA011999 Southern California Research Center for ALPD and Cirrhosis funded by NIAAA/NIH; as well as support from AGAUR of the Generalitat de Catalunya SGR-2017-1112, European Cooperation in Science & Technology (COST) ACTION CA17112 Prospective European Drug-Induced Liver Injury Network, the "ER stress-mitochondrial cholesterol axis in obesity-associated insulin resistance and comorbidities"-Ayudas FUNDACION BBVA, the Red Nacional 2018-102799-T de Enfermedades Metabólicas y Cáncer and the Project 201916/31 Contribution of mitochondrial oxysterol and bile acid metabolism to liver carcinogenesis 2019 by Fundació Marato TV3.

Author contribution

CAV, NIU, SN, LCR, ST, PSR, RF performed mouse studies, *in vitro* work and analyzed data; ST, NIU performed expression in clinical samples; CGR, JCFC, conceived the study, analyzed all data, provided financial support and supervised the study. All authors have read and agreed to the final version of the manuscript.

Data availability

The data that support the findings of this study are available from the corresponding author upon reasonable request.

Declaration of competing interest

Authors declare there are no conflicts of interest.

Acknowledgments

We are very grateful to Prof. Jose M. Mato for kindly supplying *Mat1a*$^{-/-}$ mice and to Dr. Alicia Alonso (OWL) for the performance of the lipidomic analyses.

Appendix A. Supplementary data

Supplementary data to this article can be found online at https://doi.org/10.1016/j.redox.2022.102596.

References

[1] H. Tilg, A.M. Diehl, Cytokines in alcoholic and nonalcoholic steatohepatitis, N. Engl. J. Med. 343 (20) (2000) 1467–1476, Nov, https://doi.org/10.1056/NEJM200011163432007.

[2] V. Ratziu, S. Bellentani, H. Cortez-Pinto, C. Day, G. Marchesini, A position statement on NAFLD/NASH based on the EASL 2009 special conference, J. Hepatol. 53 (2) (Aug. 2010) 372–384, https://doi.org/10.1016/j.jhep.2010.04.008.

[3] J.M. Mato, M.L. Martínez-Chantar, S.C. Lu, Methionine metabolism and liver disease, Annu. Rev. Nutr. 28 (2008) 273–293, https://doi.org/10.1146/annurev.nutr.28.061807.155438.

[4] J.M. Mato, S.C. Lu, Role of S-adenosyl-L-methionine in liver health and injury, Hepatol. Baltim. Md 45 (5) (May 2007) 1306–1312, https://doi.org/10.1002/hep.21650.

[5] V. Purohit, et al., Role of S-adenosylmethionine, folate, and betaine in the treatment of alcoholic liver disease: summary of a symposium, Am. J. Clin. Nutr. 86 (1) (Jul. 2007) 14–24.

[6] A.M. Duce, P. Ortíz, C. Cabrero, J.M. Mato, S-adenosyl-L-methionine synthetase and phospholipid methyltransferase are inhibited in human cirrhosis, Hepatol. Baltim. Md 8 (1) (Feb. 1988) 65–68, https://doi.org/10.1002/hep.1840080113.

[7] S.C. Lu, Z.Z. Huang, H. Yang, J.M. Mato, M.A. Avila, H. Tsukamoto, Changes in methionine adenosyltransferase and S-adenosylmethionine homeostasis in alcoholic rat liver, Am. J. Physiol. Gastrointest. Liver Physiol. 279 (1) (Jul. 2000) G178–G185.

[8] A.J. Barak, H.C. Beckenhauer, M.E. Mailliard, K.K. Kharbanda, D.J. Tuma, Betaine lowers elevated s-adenosylhomocysteine levels in hepatocytes from ethanol-fed rats, J. Nutr. 133 (9) (Sep. 2003) 2845–2848, https://doi.org/10.1093/jn/133.9.2845.

[9] Z. Song, et al., Alcohol-induced S-adenosylhomocysteine accumulation in the liver sensitizes to TNF hepatotoxicity: possible involvement of mitochondrial S-adenosylmethionine transport, Biochem. Pharmacol. 74 (3) (Aug. 2007) 521–531, https://doi.org/10.1016/j.bcp.2007.05.005.

[10] N. Kaplowitz, T.A. Than, M. Shinohara, C. Ji, Endoplasmic reticulum stress and liver injury, Semin. Liver Dis. 27 (4) (Nov. 2007) 367–377, https://doi.org/10.1055/s-2007-991513.

[11] C. Ji, N. Kaplowitz, Betaine decreases hyperhomocysteinemia, endoplasmic reticulum stress, and liver injury in alcohol-fed mice, Gastroenterology 124 (5) (May 2003) 1488–1499.

[12] S.C. Lu, et al., Methionine adenosyltransferase 1A knockout mice are predisposed to liver injury and exhibit increased expression of genes involved in proliferation, Proc. Natl. Acad. Sci. U.S.A. 98 (10) (May 2001) 5560–5565, https://doi.org/10.1073/pnas.091016398.

[13] L.K. Ryland, T.E. Fox, X. Liu, T.P. Loughran, M. Kester, Dysregulation of sphingolipid metabolism in cancer, Cancer Biol. Ther. 11 (2) (Jan. 2011) 138–149, https://doi.org/10.4161/cbt.11.2.14624.

[14] B. Ogretmen, Y.A. Hannun, Biologically active sphingolipids in cancer pathogenesis and treatment, Nat. Rev. Cancer 4 (8) (2004) 604–616, https://doi.org/10.1038/nrc1411, agost.

[15] S. Ponnusamy, et al., Sphingolipids and cancer: ceramide and sphingosine-1-phosphate in the regulation of cell death and drug resistance, Future Oncol. Lond. Engl. 6 (10) (2010) 1603–1624, Oct, https://doi.org/10.2217/fon.10.116.

[16] J.A. Chavez, S.A. Summers, A ceramide-centric view of insulin resistance, Cell Metabol. 15 (5) (May 2012) 585–594, https://doi.org/10.1016/j.cmet.2012.04.002.

[17] K. Hirschberg, J. Rodger, A.H. Futerman, The long-chain sphingoid base of sphingolipids is acylated at the cytosolic surface of the endoplasmic reticulum in rat liver, Biochem. J. 290 (Pt 3) (Mar. 1993) 751–757, https://doi.org/10.1042/bj2900751.

[18] J.P. Jaffrézou, et al., Daunorubicin-induced apoptosis: triggering of ceramide generation through sphingomyelin hydrolysis, EMBO J. 15 (10) (May 1996) 2417–2424.

[19] K. Kitatani, J. Idkowiak-Baldys, Y.A. Hannun, The sphingolipid salvage pathway in ceramide metabolism and signaling, Cell. Signal. 20 (6) (Jun. 2008) 1010–1018, https://doi.org/10.1016/j.cellsig.2007.12.006.

[20] Y.A. Hannun, The sphingomyelin cycle and the second messenger function of ceramide, J. Biol. Chem. 269 (5) (1994) 3125–3128, Feb.

[21] N. Insausti-Urkia, E. Solsona-Vilarrasa, C. Garcia-Ruiz, J.C. Fernandez-Checa, Sphingomyelinases and liver disease, Biomolecules 10 (11) (2020 Oct 30) 1497, https://doi.org/10.3390/biom10111497.

[22] C. García-Ruiz, M. Marí, A. Morales, A. Colell, E. Ardite, J.C. Fernández-Checa, Human placenta sphingomyelinase, an exogenous acidic pH-optimum sphingomyelinase, induces oxidative stress, glutathione depletion, and apoptosis in rat hepatocytes, Hepatology 32 (1) (2000) 56–65.

[23] A. Moles, N. Tarrats, A. Morales, M. Domínguez, R. Bataller, J. Caballería, C. García-Ruiz, J.C. Fernández-Checa, M. Marí, Acidic sphingomyelinase controls hepatic stellate cell activation and in vivo liver fibrogenesis, Am. J. Pathol. 177 (3) (2010 Sep) 1214–1224, https://doi.org/10.2353/ajpath.2010.091257.

[24] A. Fernandez, N. Matias, R. Fucho, V. Ribas, C. Von Montfort, N. Nuño, A. Baulies, L. Martinez, N. Tarrats, M. Mari, A. Colell, A. Morales, L. Dubuquoy, P. Mathurin, R. Bataller, J. Caballeria, M. Elena, J. Balsinde, N. Kaplowitz, C. Garcia-Ruiz, J. C. Fernandez-Checa, ASMase is required for chronic alcohol induced hepatic endoplasmic reticulum stress and mitochondrial cholesterol loading, J. Hepatol. 59 (4) (2013 Oct) 805–813, https://doi.org/10.1016/j.jhep.2013.05.023.

[25] R. Fucho, L. Martínez, A. Baulies, S. Torres, N. Tarrats, A. Fernandez, V. Ribas, A. M. Astudillo, J. Balsinde, P. Garcia-Rovés, M. Elena, I. Bergheim, S. Lotersztajn, C. Trautwein, H. Appelqvist, A.W. Paton, J.C. Paton, M.J. Czaja, N. Kaplowitz, J. C. Fernandez-Checa, C. García-Ruiz, ASMase regulates autophagy and lysosomal membrane permeabilization and its inhibition prevents early stage non-alcoholic steatohepatitis, J. Hepatol. 61 (5) (2014 Nov) 1126–1134, https://doi.org/10.1016/j.jhep.2014.06.009.

[26] F. Caballero, et al., Specific contribution of methionine and choline in nutritional nonalcoholic steatohepatitis: impact on mitochondrial S-adenosyl-L-methionine and glutathione, J. Biol. Chem. 285 (24) (Jun. 2010) 18528–18536, https://doi.org/10.1074/jbc.M109.099333.

[27] M. Marí, et al., Acidic sphingomyelinase downregulates the liver-specific methionine adenosyltransferase 1A, contributing to tumor necrosis factor-induced lethal hepatitis, J. Clin. Invest. 113 (6) (Mar. 2004) 895–904, https://doi.org/10.1172/JCI19852.

[28] Z. Lu, Y. Li, W.-K. Syn, Z. Wang, M.F. Lopes-Virella, T.J. Lyons, Y. Huang, Amitriptyline inhibits nonalcoholic steatohepatitis and atherosclerosis induced by high-fat diet and LPS through modulation of sphingolipid metabolism, Am. J. Physiol. Endocrinol. Metab. 318 (2020) E131–E144.

[29] K. Horinouchi, S. Erlich, D.P. Perl, K. Ferlinz, C.L. Bisgaier, K. Sandhoff, E. H. Schuchman, Acid sphingomyelinase deficient mice: a model of types A and B Niemann–Pick disease, Nat. Genet. 10 (3) (1995) 288–293.

[30] A. Bertola, S. Mathews, S.H. Ki, H. Wang, B. Gao, Mouse model of chronic and binge ethanol feeding (the NIAAA model), Nat. Protoc. 8 (3) (2013) 627–637.

[31] N.A. Osna, R.L. White, T.M. Donohue, M.R. Beard, D.J. Tuma, K.K. Kharbanda, Impaired methylation as a novel mechanism for proteasome suppression in liver cells, Biochem. Biophys. Res. Commun. 391 (2) (2010) 1291–1296.

[32] Z. Song, Z. Zhou, M. Song, S. Uriarte, T. Chen, I. Deaciuc, C.J. McClain, Alcohol-induced S-adenosylhomocysteine accumulation in the liver sensitizes to TNF hepatotoxicity: possible involvement of mitochondrial S-adenosylmethionine transport, Biochem. Pharmacol. 74 (3) (2007) 521–531.

[33] I. Martínez-Arranz, R. Mayo, M. Pérez-Cormenzana, I. Mincholé, L. Salazar, C. Alonso, J.M. Mato, Enhancing metabolomics research through data mining, J. Proteonomics (2015) 275–288.

[34] Z. Li, L.B. Agellon, T.M. Allen, M. Umeda, L. Jewell, A. Mason, D.E. Vance, The ratio of phosphatidylcholine to phosphatidylethanolamine influences membrane integrity and steatohepatitis, Cell Metabol. 3 (5) (2006 May) 321–331, https://doi.org/10.1016/j.cmet.2006.03.007.

[35] C. Garcia-Ruiz, J.M. Mato, D. Vance, N. Kaplowitz, J.C. Fernández-Checa, Acid sphingomyelinase-ceramide system in steatohepatitis: a novel target regulating multiple pathways, J Hepatol 62 (1) (2015) 219–233, https://doi.org/10.1016/j.jhep.2014.09.023.

[36] H.H. Hansen, M. Feigh, S.S. Veidal, K.T. Rigbolt, N. Vrang, K. Fosgerau, Mouse models of nonalcoholic steatohepatitis in preclinical drug development, Drug Discov. Today 22 (2017) 1707–1718.

[37] C. Alonso, D. Fernández-Ramos, M. Varela-Rey, I. Martínez-Arranz, N. Navasa, S. M. Van Liempd, J.L. Lavín Trueba, R. Mayo, C.P. Ilisso, V.G. de Juan, M. Iruarrizaga-Lejarreta, L. delaCruz-Villar, I. Mincholé, A. Robinson, J. Crespo, A. Martín-Duce, M. Romero-Gómez, H. Sann, J. Platon, J. Van Eyk, P. Aspichueta, M. Noureddin, J.M. Falcón-Pérez, J. Anguita, A.M. Aransay, M.L. Martínez-Chantar, S.C. Lu, J.M. Mato, Metabolomic identification of subtypes of nonalcoholic steatohepatitis, Gastroenterology 152 (6) (2017) 1449–1461, https://doi.org/10.1053/j.gastro.2017.01.015, e7.

[38] G.H. Werstuck, S.R. Lentz, S. Dayal, G.S. Hossain, S.K. Sood, Y.Y. Shi, R.C. Austin, Homocysteine-induced endoplasmic reticulum stress causes dysregulation of the cholesterol and triglyceride biosynthetic pathways, J. Clin. Investig. 107 (10) (2001) 1263–1273.

[39] C.A. Moylan, H. Pang, A. Dellinger, A. Suzuki, M.E. Garrett, C.D. Guy, et al., Hepatic gene expression profiles differentiate pre-symptomatic patients with mild versus severe nonalcoholic fatty liver disease, Hepatology 59 (2014) 471–482.

[40] S. Murphy, H. Yang, C.A. Moylan, H. Pang, A. Dellinger, et al., Relationship between the methylome and transcriptome in patients with nonalcoholic fatty liver disease, Gastroenterology 145 (2013) 1076–1087.

[41] A.M. Duce, P. Ortíz, C. Cabrero, J.M. Mato, S-adenosyl-L-methionine synthetase and phospholipid methyltransferase are inhibited in human cirrhosis, Hepatolgoy 8 (1988), 65-58.

[42] T. Guo, Z. Dai, K.E. You, S.-F. Battaglia-Hsu, J. Feng, F. Wang, et al., S-adenosylmethionine upregulates the angiotensin receptor-binding protein ATRAP via the methylation of HuR in NAFLD, Cell Death Dis. 12 (2021) 306.

[43] C.M. Simonaro, J.H. Park, E. Eliyahu, N. Shtraizent, M.M. McGovern, E. H. Schuchman, Imprinting at the SMPD1 locus: implications for acid sphingomyelinase-deficient Niemann-Pick disease, Am. J. Hum. Genet. 78 (5) (2006 May) 865–870.

[44] P.A. Lang, M. Schenck, J.P. Nicolay, J.U. Becker, D.S. Kempe, A. Lupescu, S. Koka, K. Eisele, B.A. Klarl, H. Rübben, K.W. Schmid, K. Mann, S. Hildenbrand, H. Hefter, S.M. Huber, T. Wieder, A. Erhardt, D. Häussinger, E. Gulbins, F. Lang, Liver cell death and anemia in Wilson disease involve acid sphingomyelinase, Nat Med 13 (2007) 164–170.

[45] A. Morales, H. Lee, F.M. Goñi, R. Kolesnick, J.C. Fernandez-Checa, Sphingolipids and cell death, Apoptosis (2007) 923–939.

[46] S.M. Turpin, H.T. Nicholls, D.M. Willmes, A. Mourier, S. Brodesser, C. M. Wunderlich, J. Mauer, E. Xu, P. Hammerschmidt, H.S. Brönneke, A. Trifunovic, G. LoSasso, F.T. Wunderlich, J.W. Kornfeld, M. Blüher, M. Krönke, J.C. Brüning, Obesity-induced CerS6-dependent C16:0 ceramide production promotes weight gain and glucose intolerance, Cell Metabol. (2014) 678–686.

[47] S. Raichur, S.T. Wang, P.W. Chan, Y. Li, J. Ching, B. Chaurasia, S. Dogra, M. K. Öhman, K. Takeda, S. Sugii, Y. Pewzner-Jung, A.H. Futerman, S.A. Summers, CerS2 haploinsufficiency inhibits β-oxidation and confers susceptibility to diet-induced steatohepatitis and insulin resistance, Cell Metabol. (2014) 687–695.

[48] N. Schiavone, P. Rosini, A. Quattrone, M. Donnini, A. Lapucci, L. Citti, A. Bevilacqua, A. Nicolin, S. Capaccioli, A conserved AU-rich element in the 3' untranslated region of bcl-2 mRNA is endowed with a destabilizing function that is involved in bcl-2 down-regulation during apoptosis, Faseb. J. (2000) 174–184.

[49] C.Y. Chen, R. Gherzi, S.E. Ong, E.L. Chan, R. Raijmakers, G.J. Pruijn, G. Stoecklin, C. Moroni, M. Mann, M. Karin, AU binding proteins recruit the exosome to degrade ARE-containing mRNAs, Cell (2001) 451–464.

[50] B.A. Bladergroen, M. Bussière, W. Klein, M.J. Geelen, L.M. Van Golde, M. Houweling, Inhibition of phosphatidylcholine and phosphatidylethanolamine biosynthesis in rat-2 fibroblasts by cell-permeable ceramides, Eur. J. Biochem. (1999) 152–160.

[51] B. Ramos, M. El Mouedden, E. Claro, S. Jackowski, Inhibition of CTP: phosphocholine cytidylyltransferase by C(2)-ceramide and its relationship to apoptosis, Mol. Pharmacol. (2002) 1068–1075.

[52] L. Videla, R. Valenzuela, Perspectives in liver redox imbalance: toxicological and pharmacological aspects underlying iron overloading, nonalcoholic fatty liver disease, and tyroid hormone action, Biofactors 48 (2022) 400–415.

[53] L. Barbier-Torres, B. Murray, J.W. Yang, J. Wang, M. Matsuda, A. Robinson, A. Binek, W. Fan, D. Fernández-Ramos, F. Lopitz-Otsoa, M. Luque-Urbano, O. Millet, N. Mavila, H. Peng, K. Ramani, R. Gottlieb, Z. Sun, S. Liangpunsakul, E. Seki, J.E. Van Eyk, J.M. Mato, S.C. Lu, Depletion of mitochondrial methionine

adenosyltransferase a1 triggers mitochondrial dysfunction in alcohol-associated liver disease, Nat. Commun. 13 (2022) 557.

[54] L.A. Videla, M.C. Hernandez-Rodas, A.H. Metherel, R. Valenzuela, Influence of the nutritional status and oxidative stress in the desaturation and elongation of n-3 and n-6 polyunsaturated fatty acids: impact on non-alcoholic fatty liver disease, Prostaglandins Leukot. Essent. Fatty Acids 181 (2022), 102441.

[55] D. Sáenz de Urturi, X. Buqué, B. Porteiro, C. Folgueira, A. Mora, T.C. Delgado, E. Prieto-Fernández, P. Olaizola, B. Gómez-Santos, M. Apodaka-Biguri, F. González-Romero, A. Nieva-Zuluaga, M. Ruiz de Gauna, N. Goikoetxea-Usandizaga, J.L. García-Rodríguez, V. Gutierrez de Juan, I. Aurrekoetxea, V. Montalvo-Romeral, E.M. Novoa, I. Martín-Guerrero, M. Varela-Rey, S. Bhanot, R. Lee, J.M. Banales, W.K. Syn, G. Sabio, M.L. Martínez-Chantar, R. Nogueiras, P. Aspichueta, Methionine adenosyltransferase 1a antisense oligonucleotides activate the liver-brown adipose tissue axis preventing obesity and associated hepatosteatosis, Nat. Commun. (2022) 1096.